Inorganic Chemistry
Article

Inorg. Chem. **2011**, *50*, 1749–1757 **1749**
DOI: 10.1021/ic102179n

Cyano-Bridged Pentanuclear and Honeycomblike $M^{III}Cu^{II}$ (M = Fe, Cr) Bimetallic Assemblies: Structural Variations Modulated by Side Groups of Macrocyclic Ligands and Magnetic Properties

Jeong Hak Lim,[†] Jung Hee Yoon,[†] Sang Yup Choi,[†] Dae Won Ryu,[†] Eui Kwan Koh,[‡] and Chang Seop Hong*,[†]

[†]*Department of Chemistry, Korea University, Seoul 136-701, Korea, and* [‡]*Nano-Bio System Research Team, Korea Basic Science Institute, Seoul 136-713, Korea*

Received October 29, 2010

Three two-dimensional (2D) layered M(III)−Cu(II) (M = Fe, Cr) bimetallic complexes and a discrete cluster were prepared using $[M(CN)_6]^{3-}$ and respective Cu macrocycles with methyl (**1**, **3**) or ethyl (**2**, **4**) side groups. The crystal structures can be described as aesthetic honeycomb-like M_2Cu_3 neutral sheets (**1**, **3**, **4**) and a pentanuclear Fe_2Cu_3 entity (**2**) with an isolated $Cu(L2)^{2+}$ moiety. The steric hindrance induced by the pendant groups renders the internal parameters of the $Cu-N_{ax}$ (where the "ax" subscript denotes axial) length and $Cu-N_{ax}-C_{ax}$ angle to become elongated and acute. The magnetic data disclose that ferromagnetic couplings are transmitted between M(III) and Cu(II) ions through the CN links. For **4**, particularly, there is a magnetically defined chain (J_c) composed of dimers (J_d) and trimers (J_t), based on the structural considerations. The intramolecular magnetic coupling constants are J_d = 3.73 cm^{-1} and J_t = 4.08 cm^{-1}, while the J_c value corresponds to 0.17 cm^{-1}. From a magnetostructural point of view, it is reasoned that the $Cu-N_{ax}$ bond length is probably a determining factor of the strength of magnetic couplings in **4**.

Introduction

Recent advances in molecule-based magnetic materials have broadened their level of interests, and the pertinent research has been extended from single magnetic characters over fascinating multiple features. To attain such materials with magnetic and other diverse properties, it would be highly desirable to elaborate a system with strong magnetic coupling and structural predictability.[1] In this vein, cyanide-bearing precursors have been frequently utilized in the construction of discrete molecules and multidimensional structures. They exhibits rich properties such as spontaneous magnetization at high critical temperature (T_C),[2] magnetochiral dichroism,[3] photomagnetic effects,[4] single-molecule magnets,[5] single-chain magnets,[6] porous magnetic metal−organic frameworks,[7] and blended dual functions.[8]

Hexacyanometallates $[A(CN)_6]^{3-}$ (where A denotes 3d metal ions) as building bricks have been extensively investigated[9] and compared to $[Fe(CN)_6]^{3-}$, the Cr(III) hexacyanide precursor is expected to promote stronger magnetic coupling, as exemplified in $\{[M(phen)(CN)_4]_2Mn(H_2O)_2\}\cdot 4H_2O$ (M = Fe, Cr) isostructural complexes where a long-range order occurs at 3.4 K for Cr(III) and 2 K for Fe(III).[10] Focusing on cyanide-bridged M(III)−Cu(II) (M = Fe, Cr) materials, target structures could be controllable by adopting paramagnetic counterparts decorated with bidentate,[2,11] tridentate,[12]

*To whom correspondence should be addressed. E-mail: cshong@korea.ac.kr.

(1) Beltran, L. M. C.; Long, J. R. *Acc. Chem. Res.* **2005**, *38*, 325.
(2) (a) Kou, H.-Z.; Gao, S.; Zhang, J.; Wen, G.-H.; Su, G.; Zheng, R. K.; Zhang, X. X. *J. Am. Chem. Soc.* **2001**, *123*, 11809. (b) Ohba, M.; Usuki, N.; Fukita, N.; Okawa, H. *Angew. Chem., Int. Ed.* **1999**, *38*, 1795.
(3) (a) Imai, H.; Inoue, K.; Kikuchi, K.; Yoshida, Y.; Ito, M.; Sunahara, T.; Onaka, S. *Angew. Chem., Int. Ed.* **2004**, *43*, 5618. (b) Inoue, K.; Imai, H.; Ghalsasi, P. S.; Kikuchi, K.; Ohba, M.; Okawa, H.; Yakhmi, J. V. *Angew. Chem., Int. Ed.* **2001**, *40*, 4242.
(4) Sato, O.; Iyoda, T.; Fujishima, A.; Hashimoto, K. *Science* **1996**, *272*, 704.
(5) (a) Sokol, J. J.; Hee, A. G.; Long, J. R. *J. Am. Chem. Soc.* **2002**, *124*, 7656. (b) Schelter, E. J.; Prosvirin, A. V.; Dunbar, K. R. *J. Am. Chem. Soc.* **2004**, *126*, 15004. (c) Lim, J. H.; Yoon, J. H.; Kim, H. C.; Hong, C. S. *Angew. Chem., Int. Ed.* **2006**, *45*, 7424.
(6) (a) Coulon, C.; Miyasaka, H.; Clérac, R. *Struct. Bonding (Berlin)* **2006**, *122*, 163. (b) Miyadaka, H.; Julve, M.; Yamashita, M.; Clérac, R. *Inorg. Chem.* **2009**, *48*, 3420. (c) Bogani, L.; Vindigni, A.; Sessoli, R.; Gatteschi *J. Mater. Chem.* **2008**, *18*, 4750. (d) Sun, H.-L.; Wang, Z.-M.; Gao, S. *Coord. Chem. Rev.* **2010**, *254*, 1081.
(7) (a) Kaye, S. S.; Long, J. R. *J. Am. Chem. Soc.* **2005**, *127*, 6506. (b) Beauvais, L. G.; Long, J. R. *J. Am. Chem. Soc.* **2002**, *124*, 12096. (c) Kurmoo, M. *Chem. Soc. Rev.* **2009**, *38*, 1353.
(8) Clemente-León, M.; Coronado, E.; López-Jordá, M.; Espallargas, G. M.; Soriano-Portillo, A.; Waerenborgh, J. C. *Chem.—Eur. J.* **2010**, *16*, 2207.
(9) Ohba, M.; Okawa, H. *Coord. Chem. Rev.* **2000**, *198*, 313.
(10) (a) Lescouëzec, R.; Lloret, F.; Julve, M.; Vaissermann, J.; Verdaguer, M.; Llusar, R.; Uriel, S. *Inorg. Chem.* **2001**, *40*, 2065. (b) Toma, L.; Lescouëzec, R.; Vaissermann, J.; Delgado, F. S.; Ruiz-Pérez, C.; Carrasco, R.; Cano, J.; Lloret, F.; Julve, M. *Chem.—Eur. J.* **2004**, *10*, 6130. (c) Zhang, Y. Z.; Gao, S.; Sun, H. L.; Su, G.; Wang, Z. M.; Zhang, S. W. *Chem. Commun.* **2004**, 1906.

Published on Web 12/30/2010

or tetradentate[13,14] ancillary ligands.[15] In case the open blocking ligands are attached, Cu(II) ions subject to a Jahn−Teller effect have donor atoms in an equatorial plane and/or axial positions. The magnetic couplings between M(III) and Cu(II) ions mediated via $Cu^{II}-N_{eq}-C_{eq}-M^{III}$ (where the subscript "eq" denotes equatorial) are moderately transmitted, relying on metric parameters.[11−14] On the other hand, M(III)−Cu(II) analogues built from Cu(II) tetradentate macrocycles could provide a good model system for a structure−magnetism correlation of $Cu^{II}-N_{ax}-C_{ax}-M^{III}$ (where the subscript "ax" denotes axial), because the octahedral Cu(II) fragments have four equatorial positions occupied by nitrogen atoms from a macrocycle and two axial sites weakly bound by facile leaving groups.[16−20] Thus, the axial binding positions are apt to be substituted by incoming bridging CN groups of $[M(CN)_6]^{3-}$ anion. In assembled M(III)−Cu(II) compounds, the magnetically important structural parameters of $Cu-N_{ax}$ lengths and/or $Cu-N_{ax}-C_{ax}$ angles can be adjusted by introducing side groups to macrocyclic ligands. To investigate a structural variation and add understanding of a magnetostructural relationship in the related molecular materials with CN groups axially coordinated to Cu ions, we attempted to devise a system by changing the length of side groups in a macrocyclic ring.

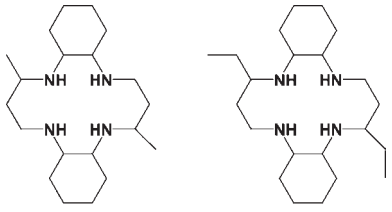

L1 L2

Herein, we report the syntheses, crystal structures, and magnetic characterizations of three honeycomb-like sheets $[Fe(CN)_6]_2[Cu(L1)]_3\cdot 6H_2O$ (**1**·$6H_2O$), $[Cr(CN)_6]_2[Cu(L1)]_3\cdot 2H_2O$ (**3**·$2H_2O$), and $[Cr(CN)_6]_2[Cu(L2)]_3\cdot 3H_2O\cdot DMF$ (**4**·$3H_2O$·DMF), as well as a pentanuclear cluster $\{[Fe(CN)_6]_2[Cu(L2)]_3\}[Cu(L2)(H_2O)_2](ClO_4)_2\cdot 4H_2O$ (**2**·$4H_2O$) obtained by assembling $[M(CN)_6]^{3-}$ (M = Fe, Cr) and $[Cu(L)(ClO_4)_2]$ (L = macrocyclic ligands, L1 and L2) with pendant groups on the macrocyclic rings. The side groups on L play a critical role in the pronounced $Cu-N_{ax}$ distances and the $Cu-N_{ax}-C_{ax}$ bendings. In particular, the significant elongation ($Cu-N_{ax}$ = 3.075 Å) around an octahedral Cu(II) center for **4** occurs, which is due to the involvement of the bulky ethyl group on L2. Magnetic measurements show that weak ferromagnetic interactions are communicated between spin centers via the CN linkage, and the magnitude of the magnetic couplings is likely governed by the $Cu-N_{ax}$ distance in the Cr(III)Cu(II) systems.

Experimental Section

Reagent. $K_3Cr(CN)_6$, macrocyclic ligands L1 and L2, $[Cu(L1)(ClO_4)_2]$, and $[Cu(L2)(ClO_4)_2]$ were prepared according to the literature procedures.[21−23] All of the other chemicals and solvents in the synthesis were of reagent grade and used as received. All manipulations were performed under aerobic conditions.

Synthesis. ***Caution!*** *Perchlorate salts of metal compounds with organic ligands are potentially explosive. Only small amounts of material should be cautiously handled.*

$[Fe(CN)_6]_2[Cu(L1)]_3\cdot 6H_2O$ (1·$6H_2O$). $K_3Fe(CN)_6$ (33 mg, 0.10 mmol) was dissolved in H_2O (8 mL) and $[Cu(L1)(ClO_4)_2]$ (90 mg, 0.15 mmol) was dissolved in DMF (7 mL). Black single crystals were formed by layering a H_2O solution of $K_3Fe(CN)_6$ at the bottom, a buffer mixed solvent of DMF/H_2O (1:1, v/v) in the middle, and a DMF solution of $[Cu(L1)(ClO_4)_2]$ on the top. Yield: 35%. Anal. Calcd for $C_{72}H_{132}Cu_3Fe_2N_{24}O_6$: C, 49.92; H, 7.68; N, 19.41. Found: C, 49.62; H, 7.66; N, 19.60.

$\{[Fe(CN)_6]_2[Cu(L2)]_3\}[Cu(L2)(H_2O)_2](ClO_4)_2\cdot 4H_2O$ (2·$4H_2O$). $K_3Fe(CN)_6$ (17 mg, 0.050 mmol) in H_2O (10 mL) was added to $[Cu(L2)(ClO_4)_2]$ (47 mg, 0.075 mmol) in MeCN (7 mL). After stirring for a few minutes, the resultant solution was slowly evaporated. Black crystals were precipitated, filtered off, and dried in air. Yield: 26%. Anal. Calcd for $C_{100}H_{188}Cu_4Fe_2N_{28}O_{14}Cl_2$: C, 49.15; H, 7.75; N, 16.05. Found: C, 49.40; H, 7.51; N, 16.48.

$[Cr(CN)_6]_2[Cu(L1)]_3\cdot 2H_2O$ (3·$2H_2O$). $K_3Cr(CN)_6$ (33 mg, 0.10 mmol) in MeOH/H_2O (1:1 v/v; 20 mL) was added to $[Cu(L1)(ClO_4)_2]$ (90 mg, 0.15 mmol) in DMF (7 mL). After stirring for a few minutes, the resultant solution was filtered and left undisturbed for several days. Violet crystals were precipitated, filtered off, and dried in air. Yield: 29%. Anal. Calcd for $C_{72}H_{124}Cr_2Cu_3N_{24}O_2$: C, 52.33; H, 7.56; N, 20.34. Found: C, 52.17; H, 7.54; N, 20.66.

$[Cr(CN)_6]_2[Cu(L2)]_3\cdot 3H_2O\cdot DMF$ (4·$3H_2O$·DMF). $K_3Cr(CN)_6$ (33 mg, 0.10 mmol) in MeOH/H_2O (1:1 v/v; 20 mL) was added to $[Cu(L2)(ClO_4)_2]$ (94 mg, 0.15 mmol) in DMF (7 mL). The resulting violet solution was filtered and left undisturbed for several days, forming violet crystals in a yield of 39%. Anal. Calcd for $C_{81}H_{145}Cr_2Cu_3N_{25}O_4$: C, 53.23; H, 8.00; N, 19.16. Found: C, 53.10; H, 7.80; N, 18.93.

Physical Measurements. Elemental analyses for C, H, and N were performed at the Elemental Analysis Service Center of Sogang University. Infrared spectra were obtained from KBr pellets with a Bomen MB-104 spectrometer. Magnetic susceptibility data for **1**−**4** were performed using a Quantum Design MPMS-7 SQUID susceptometer. Diamagnetic corrections of **1**−**4** were estimated from Pascal's Tables.

Crystallographic Structure Determination. X-ray data for **1**−**4** were collected on a Bruker SMART APEXII diffractometer that was equipped with graphite monochromated Mo Kα radiation (λ = 0.71073 Å). Preliminary orientation matrix and cell parameters were determined from three sets of ω scans at

(11) Thétiot, F.; Triki, S.; Pala, J. S.; Gómez-García, C. J.; Golhen, S. *Chem. Commun.* **2002**, 1078.
(12) Fu, D. G.; Chen, J.; Tan, X. S.; Jiang, L. J.; Zhang, S. W.; Zheng, P. J.; Tang, W. X. *Inorg. Chem.* **1997**, *36*, 220.
(13) Liu, C.-M.; Gao, S.; Kou, H.-Z.; Zhang, D.-Q.; Sun, H.-L.; Zhu, D.-B. *Cryst. Growth Des.* **2006**, *6*, 94.
(14) Marvaud, V.; Decroix, C.; Scuiller, A.; Guyard-Duhayon, C.; Vaissermann, J.; Gonnet, F.; Verdaguer, M. *Chem.—Eur. J.* **2003**, *9*, 1677.
(15) (a) Yuan, A.; Shen, X.; Zhou, H. *Transition Met. Chem.* **2008**, *33*, 133. (b) Parker, R. J.; Hockless, D. C. R.; Moubaraki, B.; Murray, K. S.; Spiccia, L. *Chem. Commun.* **1996**, 2789. (c) Ohba, M.; Okawa, H.; Fukita, N.; Hashimoto, Y. *J. Am. Chem. Soc.* **1997**, *119*, 1011. (d) Kou, H.-Z.; Liao, D.-Z.; Cheng, P.; Jiang, Z.-H.; Yan, S.-P.; Wang, G.-L.; Yao, X.-K.; Wang, H.-G. *J. Chem. Soc., Dalton Trans.* **1997**, 1503. (e) Rodríguez-Diéguez, A.; Colacio, E. *Polyhedron* **2007**, *26*, 2859.
(16) Sereda, O.; Ribas, J.; Stoeckli-Evans, H. *Inorg. Chem.* **2008**, *47*, 5107.
(17) Kou, H.-Z.; Zhou, B. C.; Si, S.-F.; Wang, R.-J. *Eur. J. Inorg. Chem.* **2004**, 401.
(18) Fallah, M. S. E.; Ribas, J.; Solans, X.; Font-Bardia, M. *New J. Chem.* **2003**, *27*, 895.
(19) Fallah, M. S. E.; Ribas, J.; Solans, X.; Font-Bardia, M. *J. Chem. Soc., Dalton Trans.* **2001**, 247.
(20) Kou, H.-Z.; Jiang, Y.-B.; Zhou, B. C.; Wang, R.-J. *Inorg. Chem.* **2004**, *43*, 3271.
(21) Cruser, F. V. D.; Miller, E. H. *J. Am. Chem. Soc.* **1906**, *28*, 1132.
(22) Kang, S.-G.; Kweon, J. K.; Jung, S.-K. *Bull. Korean Chem. Soc.* **1991**, *12*, 483.
(23) Lim, J. H.; Kang, J. S.; Kim, H. C.; Koh, E. K.; Hong, C. S. *Inorg. Chem.* **2006**, *45*, 7821.

Table 1. Crystallographic Data for **1**−**4**

	1	**2**·4H_2O	**3**	**4**
formula	$C_{72}H_{120}Fe_2Cu_3N_{24}$	$C_{100}H_{188}Fe_2Cu_4N_{28}O_{14}Cl_2$	$C_{72}H_{120}Cr_2Cu_3N_{24}$	$C_{72}H_{132}Cr_2Cu_3N_{24}$
formula weight, fw	1624.24	2443.54	1616.54	1700.70
crystal system	triclinic	triclinic	triclinic	triclinic
space group	$P\bar{1}$	$P\bar{1}$	$P\bar{1}$	$P\bar{1}$
temperature, T (K)	293	293	293	293
a (Å)	9.8567(3)	10.4644(3)	10.1330(3)	16.8660(7)
b (Å)	16.1182(5)	17.3263(4)	16.2955(4)	17.7731(8)
c (Å)	17.1430(5)	17.7839(4)	17.4383(5)	17.9983(8)
α (°)	64.3460(10)	69.6810(10)	65.0090(10)	68.3260(10)
β (°)	74.7280(10)	77.4740(10)	68.7600(10)	68.7600(10)
γ (°)	83.2070(10)	89.2570(10)	81.9440(10)	74.5930(10)
V (Å^3)	2368.35(12)	2944.92(13)	2531.63(12)	4618.7(3)
Z	1	1	1	2
d_{calc} (g cm^{-3})	1.139	1.378	1.060	1.223
μ (mm^{-1})	1.009	1.064	0.872	0.959
F(000)	859	1298	855	1806
reflections collected	39046	48191	42304	76220
unique reflections	11562	14392	12465	22632
goodness-of-fit, GOF	1.054	1.019	0.807	1.055
$R1^a$ [$I > 2\sigma(I)$]	0.0280	0.0517	0.0457	0.0500
$wR2^b$ [$I > 2\sigma(I)$]	0.0715	0.1313	0.0919	0.1244

$^a R1 = \sum||F_O| - |F_C||/\sum|F_C|$. $^b wR2 = [\sum w(F_O^2 - F_C^2)^2/\sum w(F_O^2)^2]^{1/2}$.

different starting angles. Data frames were obtained at scan intervals of 0.5° with an exposure time of 10 s per frame. The reflection data were corrected for Lorentz and polarization factors. Absorption corrections were performed using SADABS.[24] The structures were solved by direct methods and refined by full-matrix least-squares analysis, using anisotropic thermal parameters for non-hydrogen atoms with the SHELXTL program.[25] Lattice solvent molecules for **1**, **3**, and **4** are significantly disordered and could not be modeled properly; therefore, the program SQUEEZE,[26] which is part of the PLATON package[27] of crystallographic software, was used to calculate the solvent disorder area and remove its contribution to the overall intensity data. All hydrogen atoms were calculated at idealized positions and refined with the riding models. Crystallographic data and the details of data collection are listed in Table 1.

Results and Discussion

Synthesis and Characterization. The Cu(II) complexes chelated with macrocyclic ligands possess two axial sites available for incoming donor atoms of $[M(CN)_6]^{3-}$. The macrocyclic ligands used in the reactions are composed of methyl and ethyl side groups potentially functioning as steric bulkiness to coordination formations. Self-assembly of $[M(CN)_6]^{3-}$ and $[Cu(L)]^{2+}$ in a stoichiometric ratio of 2:3 generated crystalline products of **1**−**4**. The use of the different solvent pairs afforded dissimilar structures of **1** and **2**. In comparison, when the identical mixed solvents were used in the reaction of $[Cr(CN)_6]^{3-}$ and $[Cu(L)]^{2+}$, the different structural patterns resulted in **3** and **4**. Hence, it seems reasonable that the consequent structures observed in **1**−**4** are affected by the presence of the disparate side groups of L. The IR data show NH stretchings of secondary amines evident at 3249(s) cm^{-1} for **1**, 3211(s) and 3238(s) cm^{-1} for **2**, 3233(s) cm^{-1} for **3**, and 3223(s) and 3232(s) cm^{-1} for **4**, respectively.[27] The characteristic bands for perchlorate anions disappear in **1**, **3**, and **4**, suggesting completion of the reactions to form neutral coordination complexes, while **2** exhibits the characteristic Cl−O stretching centered at 1086 cm^{-1}. The CN stretching vibrations in the IR spectra are present at 2120(m) cm^{-1} for **1**, 2108(m) cm^{-1} for **2,** 2121(m) cm^{-1} for **3**, and 2114(m) cm^{-1} for **4**, similar to those of M(III)-Cu(II) complexes with long Cu−N(cyanide) distances.[15,17,19]

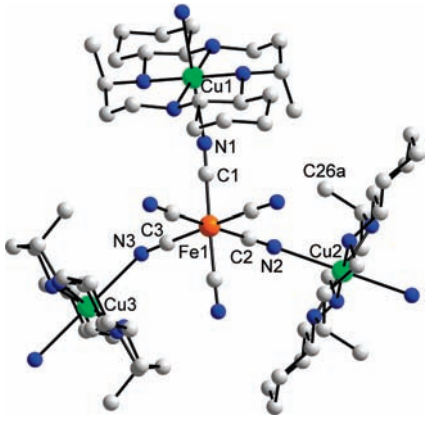

Figure 1. Molecular diagram of **1** with the atom-labeling scheme. Symmetry transformations used to generate equivalent atoms: $a = (1 - x,1 - y,1 - z)$.

Description of the Structures. Complex **1** is shown in Figure 1 with selected atom-labeling scheme. Selected bond lengths and angles are tabulated in Table 2. The Fe geometry can be described as an octahedron coordinated by six CN groups, and the bond Fe−C lengths (1.935−1.952 Å) and Fe−C−N angles with a maximum deviation of 6.0° from 180° are similar to other Fe(III) hexacyanides.[9,15] For the Cu(II) macrocyclic fragment with the methyl group, a typical Jahn−Teller distortion occurs as determined by larger axial Cu−N_{ax} bond lengths (Cu1−N1 = 2.6512(14) Å, Cu2−N2 = 2.5526(14) Å, and Cu3−N3 = 2.6535(13) Å) than equatorial Cu−N_{eq} distances

(24) Sheldrick, G. M. *SADABS, A Program for Area Detector Absorption Corrections*; University of Göttingen: Göttingen, Germany, 1994.
(25) Sheldrick, G. M. *SHELXTL,* version 5; Bruker AXS: Madison, WI, 1995.
(26) van der Sluis, P.; Spek, A. L. *Acta Crystallogr., Sect. A: Found. Crystallogr.* **1990**, *A46*, 194.
(27) Spek, A. L. *Acta Crystallogr., Sect. A: Found. Crystallogr.* **1990**, *A46*, 1.

Table 2. Selected Bond Lengths and Bond Angles for **1** and **2**[a]

For Compound **1**

Bond Lengths

Fe(1)−C(1)	1.9386(14) Å	Fe(1)−C(2)	1.9345(14) Å
Fe(1)−C(3)	1.9424(13) Å	Fe(1)−C(4)	1.9519(14) Å
Fe(1)−C(5)	1.9455(13) Å	Fe(1)−C(6)	1.9479(13) Å
Cu(1)−N(1)	2.6512(14) Å	Cu(2)−N(2)	2.5526(14) Å
Cu(3)−N(3)	2.6535(13) Å	Cu(1)−N(7)	2.0228(11) Å
Cu(1)−N(8)	2.0383(12) Å	Cu(2)−N(9)	2.0217(10) Å
Cu(2)−N(10)	2.0537(10) Å	Cu(3)−N(12)	2.0199(11) Å
Cu(3)−N(11)	2.0432(12) Å		

Bond Angles

N(1)−C(1)−Fe(1)	179.06(15)°	N(2)−C(2)−Fe(1)	173.97(12)°
N(3)−C(3)−Fe(1)	176.69(12)°	N(4)−C(4)−Fe(1)	178.58(12)°
N(5)−C(5)−Fe(1)	175.57(12)°	N(6)−C(6)−Fe(1)	177.58(12)°
C(1)−N(1)−Cu(1)	129.48(13)°	C(2)−N(2)−Cu(2)	136.74(12)°
C(3)−N(3)−Cu(3)	132.08(11)°		

For Compound **2**

Bond Lengths

Fe(1)−C(1)	1.935(4) Å	Fe(1)−C(2)	1.957(4) Å
Fe(1)−C(3)	1.950(5) Å	Fe(1)−C(4)	1.938(4) Å
Fe(1)−C(5)	1.940(4) Å	Fe(1)−C(6)	1.956(4) Å
Cu(1)−N(1)	2.245(3) Å	Cu(2)−N(2)	2.758(5) Å
Cu(3)−O(6*d*)	2.693(10) Å	Cu(1)−N(9)	2.022(3) Å
Cu(1)−N(7)	2.026(3) Å	Cu(1)−N(8)	2.045(3) Å
Cu(1)−N(10)	2.085(3) Å	Cu(2)−N(14)	2.015(3) Å
Cu(2)−N(13)	2.046(3) Å	Cu(3)−N(12)	2.019(3) Å
Cu(3)−N(11)	2.037(3) Å		

Bond Angles

N(1)−C(1)−Fe(1)	176.8(3)°	N(2)−C(2)−Fe(1)	171.9(4)°
N(3)−C(3)−Fe(1)	176.0(5)°	N(4)−C(4)−Fe(1)	178.5(5)°
N(5)−C(5)−Fe(1)	176.2(3)°	N(6)−C(6)−Fe(1)	176.7(4)°
C(1)−N(1)−Cu(1)	148.6(3)°	C(2)−N(2)−Cu(2)	130.6(4)°

[a] Symmetry transformations used to generate equivalent atoms: d = $(1-x,1-y,1-z)$.

(2.0199−2.0537 Å). Note that the methyl (C26*a*; a = $(1-x,1-y,1-z)$) group of L1 sits like a fence toward the hexacyanide and pushes it back, eventually leading to the elongated Cu−N_{ax} distances in the apical directions. Moreover, to reduce steric hindrance, the Cu−N_{ax}−C_{ax} skeleton is bent in the midway of the methyl fence (see Figure S1 in the Supporting Information). The angles for Cu and bridging CN groups are 129.48(11)° for Cu1−N1−C1, 136.74(11)° for Cu2−N2−C2, and 132.08(11)° for Cu3−N3−C3. The metal−metal distances through the CN bridges are 5.1865(2) Å for Fe1−Cu1, 5.1700(2) Å for Fe1−Cu2, and 5.2142(2) Å for Fe1−Cu3.

Figure 2 shows a 2D honeycomb-like architecture, which is also found in those of hexacyanometallate- or octacyanometallate-based bimetallic systems.[9,28,29] The Fe(III) atoms are positioned at the corners of a hexagon and Cu(II) macrocyclic moieties constitute the edges of the hexagon. The dimension of the hexagon is that the edge distances between Fe atoms are in the range from

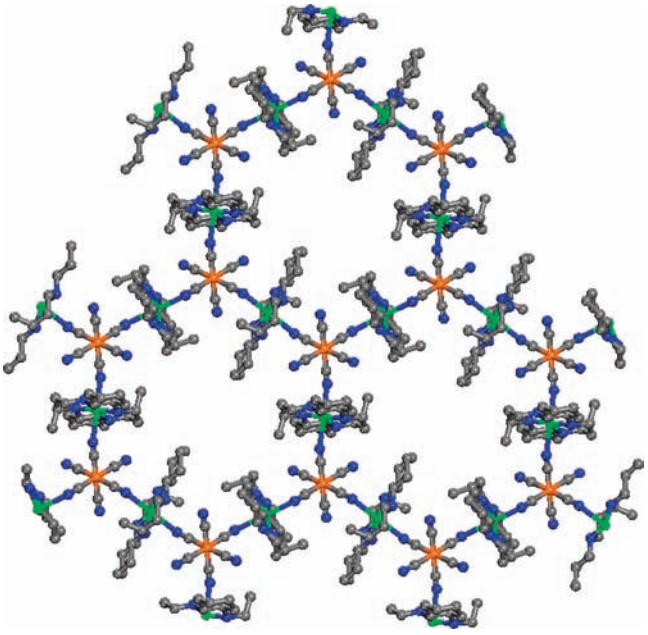

Figure 2. Two-dimensional (2D) extended layer structure of **1**, illustrating a honeycomb-like structure. (C atoms are presented in gray, N atoms are presented in blue, Cu atoms are presented in green, and Fe atoms are presented in orange.)

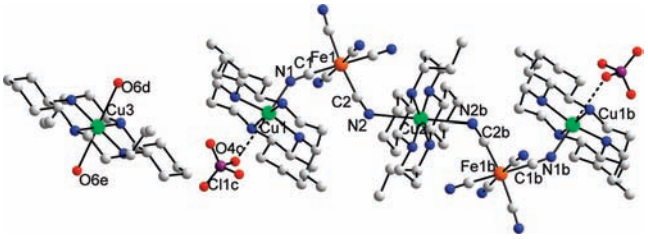

Figure 3. Molecular diagram of **2** with the atom-labeling scheme. Symmetry transformations used to generate equivalent atoms: b = $(2-x,2-y,-z)$; c = $(1+x,y,z)$; d = $(1-x,1-y,1-z)$; e = $(x,-1+y,z)$.

10.340 Å to 10.428 Å and the diagonal Fe centers in the same hexagon are separated with distances from 20.128 Å to 20.917 Å. The layered structure is manifested by the side view (see Figure S2 in the Supporting Information). The shortest interlayer Fe−Cu distances are 7.940 Å.

The structure of **2** is shown in Figure 3. Selected bond lengths and angles are given in Table 2. The pentanuclear Cu_3Fe_2 cluster is completed by the coordination of perchlorate anions to the axial sites of the terminal Cu(II) ions, and the isolated $[Cu(L2)(H_2O)_2]^{2+}$ cation is present in the structure to maintain charge balance. The Fe−C distances range from 1.935 Å to 1.957 Å, while the Fe−C−N angles are quite linear, with a maximum deviation of 8.1° for Fe1−C2−N2. The Cu2 atom is encircled by four equatorial N atoms from L2 and two axial N atoms from CN ligands. The axial Cu2−N2 length is 2.758(4) Å and the related Cu2−N2−C2 angle is 130.6(3)°. In comparison, the Cu1−N1 length is relatively short, 2.245(3) Å, much smaller than the Cu2−N2 length in **2** and the respective lengths in **1**. Contrary to the Cu1−N1 length, the Cu1−O4*c* (c = $(1+x,y,z)$) interaction in the opposite side of the Cu1−N1 coordination bond is extremely weak (3.095(8) Å). Interestingly, the local structure around Cu1 indicates that the metal center resides slightly away from

(28) Lim, J. H.; You, Y. S.; Yoo, H. S.; Yoon, J. H.; Kim, J. I.; Koh, E. K.; Hong, C. S. *Inorg. Chem.* **2007**, *46*, 10578.
(29) (a) Kou, H.-Z.; Gao, S.; Bai, O.; Wang, Z.-M. *Inorg. Chem.* **2001**, *40*, 6287. (b) Ohba, M.; Okawa, H.; Fukita, N.; Hashimoto, Y. *J. Am. Chem. Soc.* **1997**, *119*, 1011. (c) Hong, C. S.; You, Y. S. *Inorg. Chim. Acta* **2004**, *357*, 3271.

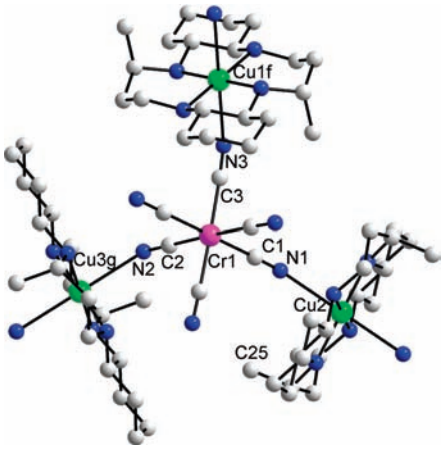

Figure 4. Molecular diagram of **3** with the atom-labeling scheme. Symmetry transformations used to generate equivalent atoms: f = $(x,1+y,z)$ and g = $(1+x,y,z)$.

the equatorial N_4 plane of L2 toward Fe1 (see Figure S3 in the Supporting Information), which is responsible for the abnormal structural metric parameters. The Cu3 atom undergoes a Jahn−Teller distortion with the axial Cu3−O6d (d = $(1-x,1-y,1-z)$) length of 2.693(10) Å. The metal−metal distances are 5.1057(7) Å for Fe1−Cu1, 5.2213(4) Å for Fe1−Cu2, and 9.0443(4) Å for Cu1−Cu3.

A molecular diagram of **3** is illustrated in Figure 4 with the selected atom-numbering scheme. Selected bond distances and angles are summarized in Table 3. The Cr center is surrounded by six CN groups with an average Cr−C bond length of 2.074(9) Å. The Cr−C−N angles are quite linear and the maximal deviation of the angles from 180° is 7.6°. Three of the six CN groups are weakly bound to axial sites of neighboring Cu(II) ions [Cu1f−N3 = 2.653(3) Å, Cu2−N1 = 2.607(3) Å, and Cu3g−N2 = 2.556(3) Å; f = $(x,1+y,z)$, g = $(1+x,y,z)$]. The obvious tetragonal elongation, compared with bond lengths between Cu ions and equatorial N atoms spanning from 2.014 Å to 2.048 Å, accounts for a Jahn−Teller effect of an octahedral Cu(II) ion. The current Cu−N_{ax} distances are rather long, but they are consistent with those found in other cyanometallate-based Cr(III)−Cu(II) families[16−20] (for instance, $[Cu(L^5)Cr(CN)_6]_6[\{Cu(L^5)(H_2O)\}_6Cr(CN)_6](ClO_4)_3\cdot 6H_2O$ (L^5 = 3,7-bis(2-aminoethyl)-1,3,5,7-tetraazabicyclo[3.3.2]decane)).[17] As for **1**, the methyl (C25) group of L1 in **3** serves as a bulky pendant and affect bending patterns in the bridging routes (see Figure S4 on the Supporting Information). The bridging Cu−N−C angles are similar: 131.8° for Cu1f−N3−C3, 133.6° for Cu2−N1−C1, and 135.6° for Cu3g−N2−C2. The Cr−Cu distances via the bridging ligands are 5.3145(1) Å for Cr1−Cu1f, 5.3101(2) Å for Cr1−Cu2, and 5.2537(1) Å for Cr1−Cu3g. Figure 5 depicts the intriguing 2D honeycomb-like structure, as shown in **1**. The edge distances between Cr atoms span from 10.507 Å to 10.629 Å, and the diagonal Cr−Cr distances range from 20.737 Å to 20.987 Å. The shortest interlayer M−Cu distances are 8.120 Å (see Figure S5 in the Supporting Information).

A molecular diagram of **4** is shown in Figure 6 with a selected atom-numbering scheme. Selected bond distances and angles are tabulated in Table 3. In the crystal structure, each Cr(III) atom is coordinated by six CN ligands and the Cr−C distances range from 2.067 Å to 2.097 Å. The respective Cr−C−N angles are almost linear, with a maximal deviation from 180° of 6.1°. For the Cu(II) fragment, a typical Jahn−Teller effect occurs, as judged by the short equatorial Cu−N_{eq} distances [average Cu−N_{eq} = 2.03(1) Å] and the long axial Cu−N_{ax} lengths.[30] The relatively short Cu−N_{ax} distances are equal to 2.456(2) Å for Cu2−N5, 2.490(2) Å for Cu3−N1, 2.481(2) Å for Cu1i−N7h (h = $(x,y,-1+z)$ and i = $(x,1+y,-1+z)$), while the longer Cu−N_{ax} lengths are 2.699(2) Å for Cu1−N4 and 2.821(2) Å for Cu3−N9h. Note that the Cu2−N8 bond is significantly weak and its separation is substantial, 3.075(3) Å, which is compatible with those reported for some cyanide-bridged Cr(III)−Cu(II) analogues.[16−20] Based on the bond lengths, the Cr_2Cu_3 unit can be virtually viewed as a combination of a trimer of Cu2−N5−C5−Cr1−C1−N1−Cu3 and a dimer of Cr2h−C7h−N7h−Cu1i. The bonding angles of Cu−N−C within the trimeric subunit are similar—143.3° for Cu2−N5−C5 and 142.3° for Cu3−N1−C1—whereas the

Table 3. Selected Bond Lengths and Bond Angles for **3** and **4**[a]

For Compound **3**

Bond Lengths

Cr(1)−C(1)	2.073(3) Å	Cr(1)−C(2)	2.059(3) Å
Cr(1)−C(3)	2.084(3) Å	Cr(1)−C(4)	2.083(3) Å
Cr(1)−C(5)	2.075(3) Å	Cr(1)−C(6)	2.068(3) Å
Cu(2)−N(1)	2.607(3) Å	Cu(1f)−N(3)	2.653(3) Å
Cu(3g)−N(2)	2.556(3) Å	Cu(1)−N(7)	2.037(2) Å
Cu(1)−N(8)	2.024(2) Å	Cu(2)−N(10)	2.018(2) Å
Cu(2)−N(9)	2.029(2) Å	Cu(3)−N(11)	2.0480(18) Å
Cu(3)−N(12)	2.0134(19) Å		

Bond Angles

N(1)−C(1)−Cr(1)	176.2(3)°	N(2)−C(2)−Cr(1)	172.4(2)°
N(3)−C(3)−Cr(1)	175.6(3)°	C(1)−N(1)−Cu(2)	133.6(3)°
C(2)−N(2)−Cu(3g)	135.7(3)°	C(3)−N(3)−Cu(1f)	131.9(3)°

For Compound **4**

Bond Lengths

Cr(1)−C(1)	2.092(2) Å	Cr(1)−C(2)	2.067(2) Å
Cr(1)−C(3)	2.102(3) Å	Cr(1)−C(4)	2.078(2) Å
Cr(1)−C(5)	2.092(2) Å	Cr(1)−C(6)	2.075(3) Å
Cu(3)−N(1)	2.490(2) Å	Cu(1)−N(4)	2.699(2) Å
Cu(2)−N(5)	2.456(2) Å	Cu(1i)-N(7)	2.481(2) Å
Cu(3)−N(9h)	2.821(2) Å	Cu(2)−N(8)	3.075(3) Å
Cu(1)−N(13)	2.0180(18) Å	Cu(1)−N(15)	2.0249(18) Å
Cu(1)−N(14)	2.0423(18) Å	Cu(1)−N(16)	2.0495(18) Å
Cu(2)−N(17)	2.019(2) Å	Cu(2)−N(18)	2.029(2) Å
Cu(2)−N(19)	2.030(2) Å	Cu(2)−N(31)	2.041(2) Å
Cu(3)−N(23)	2.0051(19) Å	Cu(3)−N(24)	2.0509(18) Å
Cu(3)−N(22)	2.0572(19) Å	N(21)−Cu(3)	2.0112(19) Å

Bond Angles

N(1)−C(1)−Cr(1)	173.9(2)°	N(4)−C(4)−Cr(1)	178.9(2)°
N(5)−C(5)−Cr(1)	176.4(2)°	C(1)−N(1)−Cu(3)	142.3(2)°
C(4)−N(4)−Cu(1)	127.9(2)°	C(5)−N(5)−Cu(2)	142.3(2)°

[a] Symmetry transformations used to generate equivalent atoms: f = $(x,1+y,z)$; g = $(1+x,y,z)$; h = $(x,y,-1+z)$; i = $(x,1+y,-1+z)$.

(30) (a) You, Y. S.; Kim, D.; Do, Y.; Oh, S. J.; Hong, C. S. *Inorg. Chem.* **2004**, *43*, 6899. (b) Shen, X.-P.; Gao, S.; Yin, G.; Yu, K.-B.; Xu, Z. *New. J. Chem.* **2004**, *28*, 996.

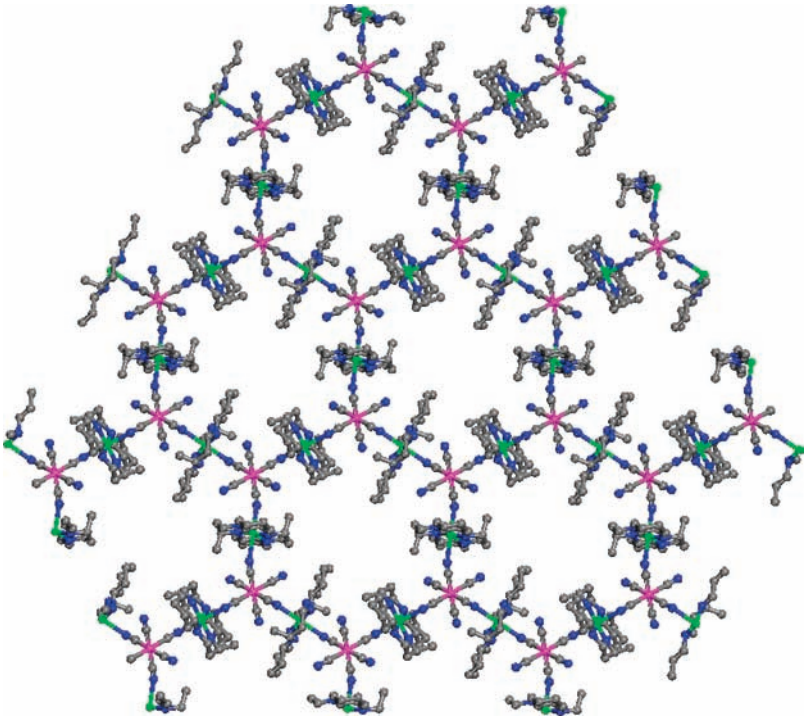

Figure 5. Two-dimensional (2D) extended layer structure of **3**, illustrating a honeycomb-like structure. (C atoms are presented in gray, N atoms are presented in blue, Cu atoms are presented in green, and Cr atoms are presented in pink.)

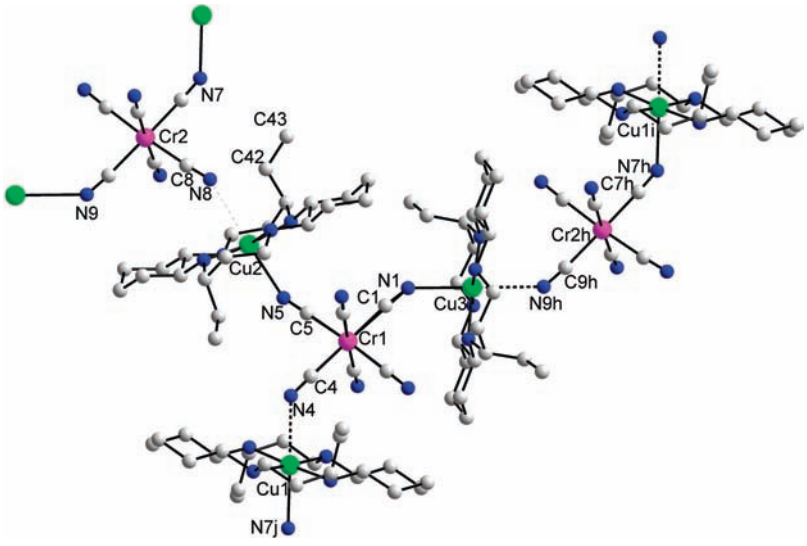

Figure 6. Molecular view of **4** with the atom-labeling scheme. Symmetry transformations used to generate equivalent atoms: $h = (x,y,-1+z)$; $i = (x,1+y,-1+z)$; $j = (x,-1+y,z)$.

angles within the dimeric entity are 132.4° for Cu1*i*−N7*h*−C7*h*, which is smaller than those of the trinuclear cluster. The molecular subunits are connected to generate a one-dimensional (1D) chain structure in which the Cu−N−C angles are 127.9° for Cu1−N4−C4 and 140.3° for Cu3−N9*h*−C9*h*. The Cr−Cu distances range from 5.187 Å to 5.748 Å. The presence of the side groups of L2 in **4** allows for the bending of $Cu-N_{ax}-C_{ax}$ in the same fashion as the previous complexes (see Figure S6 in the Supporting Information). Note that the ethyl (C42−C43) group of L2 is bulkier than the methyl group of L1, which explains the apparent structural variation. The $Cu-N_{ax}$ bonds (mean length = 2.48(2) Å) within the clusters are rather stronger than the other bonds (larger than 2.699 Å). This is because the CN group (C7−N7) is oriented nearby the pendant ethyl side group, giving rise to a severe steric effect (see Figure S7 in the Supporting Information). Accordingly, the more-enhanced elongation of the corresponding $Cu-N_{ax}$ bonds in **4** than that of **3** is associated with the influence of the bulky ethyl (C42−C43) side groups of L2 on the structural consequence.

The extended structure of **4** can be seen as a quasi-honeycomb-like structure, as illustrated in Figure 7. Because of the presence of the ethyl group on L2, the hexagon is formed via very weak coordination powers. The edge distances in **4** are mostly longer than those in **3**,

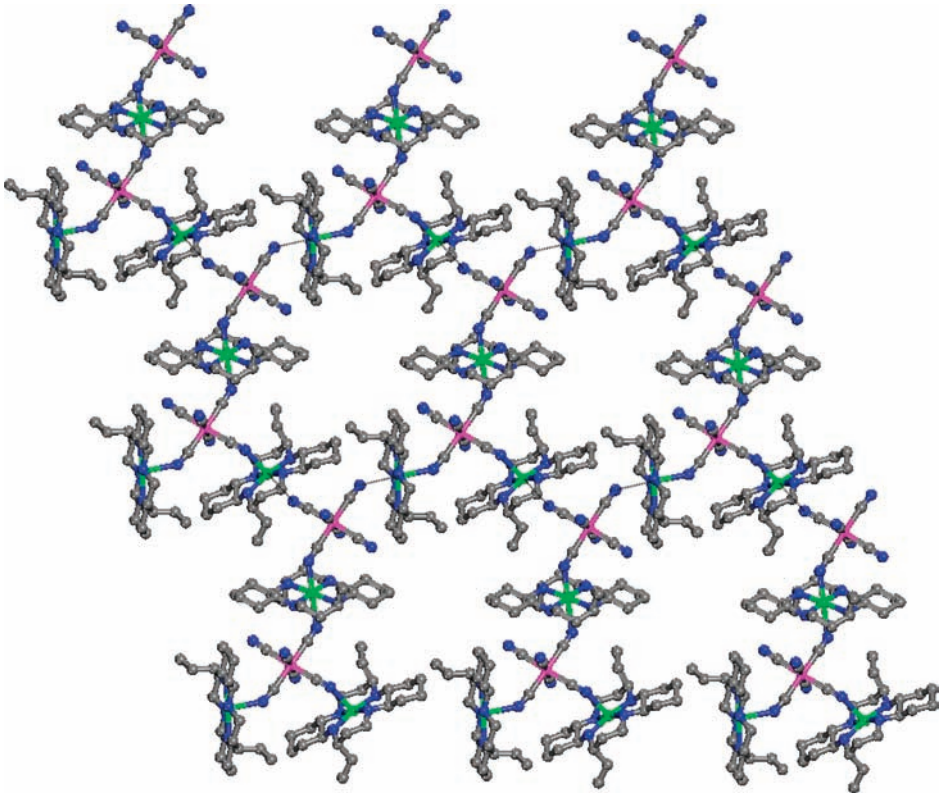

Figure 7. Extended layer structure of **4**, showing a quasi-honeycomb-like structure.

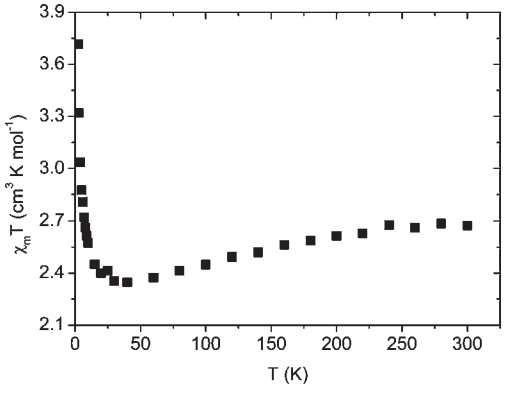

Figure 8. Plot of $\chi_m T$ vs T for **1**.

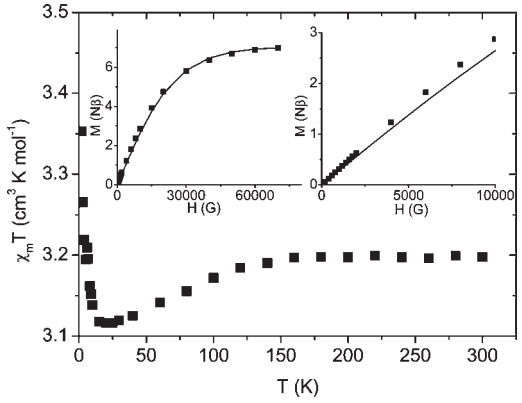

Figure 9. Plot of $\chi_m T$ vs T for **2**. The insets present the field dependence of the magnetization at 2 K. The solid line indicates the Brillouin curve deduced from noncoupled four Cu(II) and two Fe(III) ions.

spanning from 10.485 Å to 11.133 Å, and the diagonal distances are in the range of 18.526−23.032 Å.

Magnetic Properties. The thermal variations of the magnetic susceptibility data for **1** and **2** were recorded at 1000 G, as plotted in Figures 8 and 9. At 300 K, the $\chi_m T$ value per Fe_2Cu_3 for **1** is 2.67 cm^3 K mol^{-1} and the value per Fe_2Cu_4 for **2** is 3.20 cm^3 K mol^{-1}. The average g values are calculated to be $g = 2.39$ for both cases, which are due to the presence of octahedral Fe(III) ions with an orbital contribution to the magnetic moment.[31,32] As the temperature is lowered, $\chi_m T$ tends to decrease. This behavior is related to the thermal change of the low-spin octahedral Fe(III) atoms ($^2T_{2g}$ ground state) with the spin−orbit coupling effects, as observed in a ferricyanide-based Fe(III)Cu(II) chain.[32] The increase in $\chi_m T$ at low temperature is consistent with weak ferromagnetic coupling between Fe(III) and Cu(II) spins. To confirm the ferromagnetic character, the $M(H)$ data for **2** were collected at 2 K, as depicted in the insets of Figure 9. The Brillouin curve is drawn based on noncoupled two Fe(III) and four Cu(II) spins with the obtained g-value. At the low-field range, the experimental data reside higher than the calculated plot, demonstrating the operation of overall ferromagnetic interactions. The long Cu−N_{ax} lengths cause the overlap between Fe $d\pi$ and Cu $d_{x^2-y^2}$ magnetic orbitals to be minimal, favoring the ferromagnetic communication through CN bridges. Similar results were also demonstrated in Fe(III)Cu(II) or M(V)Cu(II) (M = Mo, W) bimetallic systems bearing axially elongated Cu(II) ions.[28,32]

(31) Shatruk, M.; Chambers, K. E.; Prosvirin, A. V.; Dunbar, K. R. *Inorg. Chem.* **2007**, *46*, 5155.
(32) Rodríguez-Diéguez, A.; Kivekäs, R.; Sillanpää, R.; Cano, J.; Lloret, F.; McKee, V.; Stoeckli-Evans, H.; Colacio, E. *Inorg. Chem.* **2006**, *45*, 10537.

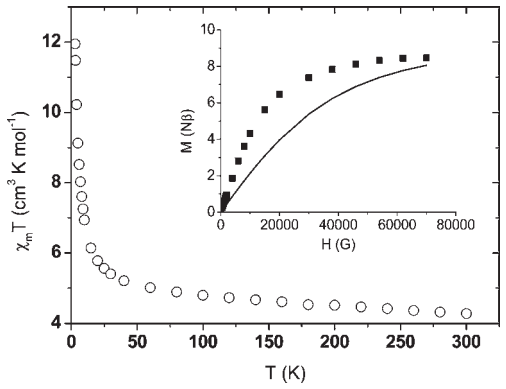

Figure 10. Plot of $\chi_m T$ vs T for **3**. The inset denotes the field dependence of the magnetization at 4 K. The solid line shows the Brillouin curve calculated from independent three Cu(II) and two Cr(III) ions.

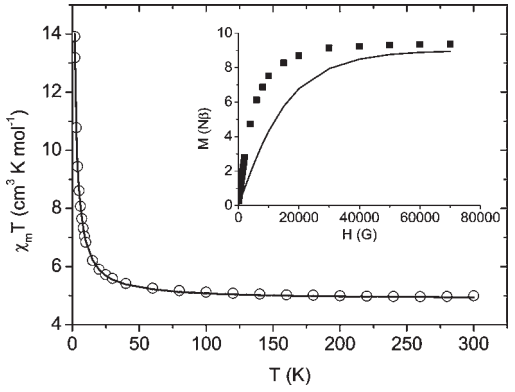

Figure 11. Plot of $\chi_m T$ vs T for **4**. The solid line in the main panel indicates the best fit of magnetic data to the proper magnetic model. The inset shows the field dependence of the magnetization at 1.8 K. The solid line in the inset represents the Brillouin curve for isolated three Cu(II) and two Cr(III) ions.

The temperature-dependent magnetic data for **3** were measured at 1000 G (see Figure 10). The room-temperature $\chi_m T$ value of 4.28 cm^3 K mol^{-1} is similar to the spin-only value of 4.88 cm^3 K mol^{-1} expected from noninteracting two Cr(III) ions ($S_{Cr} = {}^3/_2$) and three Cu(II) ions ($S_{Cu} = {}^1/_2$). The $\chi_m T$ product increases slowly and abruptly as the temperature is reduced. This magnetic behavior can be interpreted by ferromagnetic interactions between paramagnetic centers mediated by bridging CN ligands. The fit of the magnetic data to the Curie−Weiss equation $[\chi_m = C/(T - \theta)]$ at $T > 80$ K gives $C = 4.27$ cm^3 K mol^{-1} and $\theta = 16.2$ K (see Figure S8 in the Supporting Information). The positive Weiss constant denotes the existence of overall ferromagnetic couplings among two types of spin centers. The ferromagnetic nature in this system is confirmed by the $M(H)$ curve in the inset of Figure 10. The experimental data lie above the curve derived by the Brillouin function with a paramagnetic combination of $2S_{Cr}$ and $3S_{Cu}$, indicating the clear evidence of ferromagnetic correlation among metal centers.

The magnetic susceptibility data for **4** were collected at 1000 G and plotted in Figure 11. The $\chi_m T$ value of 4.99 cm^3 K mol^{-1} at 300 K corresponds to the theoretical one anticipated from isolated paramagnetic centers. Upon cooling, $\chi_m T$ undergoes a steady rise and then a sharp increase as in **3**. Ferromagnetic couplings between magnetic

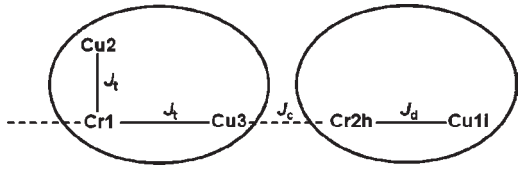

Figure 12. Schematic representation of magnetic exchange couplings in **4**. The solid lines represent intradimer (J_d) and intratrimer (J_t) interactions, and the dotted lines represent intercluster interactions (J_c).

centers are operative as manifested by the Curie−Weiss fitting at $T > 20$ K with $C = 4.91$ cm^3 K mol^{-1} and $\theta = 3.8$ K (see Figure S9 in the Supporting Information). The $M(H)$ data at 1.8 K for **4** definitely support the presence of global ferromagnetic couplings because the calculated Brillouin curve for noncoupled paramagnetic centers is lower than the magnetization data in the entire field range (inset of Figure 11).

With reference to the structural data of **4**, the magnetic coupling scheme can be analyzed as a dimeric and a trimeric subunit. The subunits are mutually interconnected via tiny coordination forces, constructing a 1D chain system. We considered a magnetic model for the dinuclear Cu1i−Cr2h skeleton with the Hamiltonian $\boldsymbol{H} = -J_d(S_{Cu1i}S_{Cr2h}) + g\beta H(S_{Cu1i} + S_{Cr2h})$ and for the trinuclear Cu2−Cr1−Cu3 route with $\boldsymbol{H} = -J_t(S_{Cu2}S_{Cr1} + S_{Cr1}S_{Cu3}) + g\beta H(S_{Cu2} + S_{Cr1} + S_{Cu3})$. The formula for molar magnetic susceptibility of the molecules can be expressed as $\chi_{molecule} = \{Ng^2\beta^2/(3kT)][\sum_S S(S+1)(2S+1)\exp(-E[S]/(kT))]\}/[\sum_S(2S+1)\exp(-E(S)/kT)]$, where $E(S)$ is eigenvalues of $\boldsymbol{H}$.

$$\chi_d = \left(\frac{Ng_d{}^2\beta^2}{3kT}\right)S_d(S_d+1) = \left(\frac{Ng_d{}^2\beta^2}{3kT}\right)[A/B] \quad (1)$$

where

$$A = 6 + 30\exp\left(\frac{2J_d}{kT}\right), \quad B = 3 + 5\exp\left(\frac{2J_d}{kT}\right)$$

and

$$\chi_t = \left(\frac{Ng_t{}^2\beta^2}{3kT}\right)S_t(S_t+1) = \left(\frac{Ng_t{}^2\beta^2}{3kT}\right)[C/D] \quad (2)$$

where

$$C = 3 + 30\exp\left(\frac{1.5J_t}{kT}\right) + 30\exp\left(\frac{2.5J_t}{kT}\right) + 105\exp\left(\frac{4J_t}{kT}\right), \quad D = 4 + 8\exp\left(\frac{1.5J_t}{kT}\right) + 8\exp\left(\frac{2.5J_t}{kT}\right) + 12\exp\left(\frac{4J_t}{kT}\right)$$

As schematized in Figure 12, which displays magnetic coupling routes, an analytical expression for a regular chain system ($H = -J\sum_i{}^{2n}S_i \cdot S_{i+1}$) was employed to examine the magnetic exchange couplings in **4**.[33] In this case, we

(33) Drillon, M.; Coronado, E.; Beltran, D.; Georges, R. *Chem. Phys.* **1983**, *79*, 449.

Table 4. Structural and Magnetic Parameters for Cyanometallate-Based Cr(III)−Cu(II) Systems with Axial or Equatorial Bridging Modes around Cu Ions[a]

compound	Cu−N_{ax} (Å)	Cu−N_{ax}−C_{ax} (°)	J (cm^{-1})	ref
$[Cu(L^3)_2]_3[Cr(CN)_6]_2\cdot 4.75H_2O$	2.595−2.671	126.3−131.3	1.64	15
$[CuL^5Cr(CN)_6]_6[\{CuL^5(H_2O)\}_6Cr(CN)_6](ClO_4)_3\cdot 6H_2O$	2.506	142.7	2.40	16
4	2.445, 2.490	142.3, 143.4	3.73	this work
	2.481	132.4	4.08	this work
$[Cu(cyclam)]_3[Cr(CN)_6]_2\cdot 4H_2O$	2.474, 2.607	132.6, 136.9	4.33	17
$[Cu(L^4)][Cu(L^4)Cr(CN)_6]\cdot ClO_4\cdot 2H_2O$	2.582	138.5	4.82	18
$\{[Cu_2(L^6)]_2[Cr(CN)_6]\}[Cr(CN)_6](ClO_4)_2$	2.297, 2.327	148.8, 150.3	22	19
$\{[Cu_2(L^6)][Cr(CN)_6][Cu(L^7)]\}^{3+}$	2.370	138.6	38.0	19

compound	Cu−N_{eq} (Å)	Cu−N_{eq}−C_{eq} (°)	J (cm^{-1})	ref
$[Cu(EtOH)_2][Cu(en)]_2[Cr(CN)_6]_2$			6.0	2a
$[(Cu(dien))_2Cr(CN)_6][Cu(dien)(H_2O)Cr(CN)_6]\cdot 4H_2O$	1.975, 1.99	172 (ave.)	12.82, 14.48	12
$[Cu(2,2'\text{-dpa})]_3[Cr(CN)_6]_2\cdot 3H_2O$	1.938, 1.978	177.7, 178.3	16.2	13
$[\{Cu(edma)\}_3Cr(CN)_6]$	1.941	168	18.32	12
$[Cr\{CN\text{-}Cu(tren)\}_6](ClO_4)_9$	1.97	176.5	45.5	14

[a] The J parameters in the $2J$ scheme were converted to those in the J scheme. L^3 = *trans*-cyclohexane-(1R,2R)-diamine, L^4 = meso-5,5,7,12,12,14-hexamethyl-1,4,8,11-tetraazacyclotetradecane, L^5 = 3,7-bis(2-aminoethyl)-1,3,5,7-tetraazabicyclo[3.3.2]decane, en = ethylenediamine, dien = diethylenetriamine, 2,2′-dpa = 2,2′-dipicolylamine, edma = ethylenediaminemonoacetate, tren = tris(2-amino)ethylamine.

treated the dinuclear and trinuclear moieties as classical spins (S_d and S_t).[28,34]

$$\chi_m T = \frac{N\beta^2}{3k}\left[g^2\left(\frac{1+u}{1-u}\right) + \delta^2\left(\frac{1-u}{1+u}\right)\right] \qquad (3)$$

The parameters are as follows: $g_d^e = g_d[S_d(S_d+1)]^{1/2}$, $g_t^e = g_t[S_t(S_t+1)]^{1/2}$, $J^e = J_c[S_d(S_d+1)S_t(S_t+1)]^{1/2}$, $g = (g_{Mn}^e + g_{Fe}^e)/2$, $\delta = (g_d^e - g_t^e)/2$, $u = \coth[J^e/(kT)] - (kT/J^e)$. Using this rough model, the magnetic data were simulated to give least-squares fitting results of $g_d = g_t = 2.0$, $J_d = 3.73\ cm^{-1}$, $J_t = 4.08\ cm^{-1}$, and $J_c = 0.17\ cm^{-1}$. The magnetic curve is well-reproduced by the estimated parameters, and the observed intracluster J_d and J_t are comparable to those of Cr−Cu bimetallic complexes ($J = 1.64-4.82\ cm^{-1}$) with Cu−N_{ax} lengths of 2.5−2.7 Å.[16−19] The intercluster J_c value is much weaker than the intracluster ones because of the long Cu−N_{ax} separations of larger than 2.7 Å. In general, the trivial magnetic strengths are transmitted through the long axial Cu−N_{ax} routes. This can be compared with the equatorial Cu−N_{eq}−C_{eq}−Cr pathways exhibiting J in the range of 6−45.5 cm^{-1}, which is concerned with short Cu−N_{eq} distances, along with orbital orthogonality.[11−14]

The total exchange coupling constant (J) results from a summation of ferromagnetic (J_F) and antiferromagnetic (J_{AF}) contributions.[35] The overall ferromagnetic consequence [$J = J_F + J_{AF} = 2k\,(>0) + 4\beta S\,(<0)$] will emerge when J_F is larger than J_{AF} proportional to the orbital integral S. In the case of equatorial Cu−N_{eq} routes, the $d_{x^2-y^2}$ orbital is oriented along the axial bond directions, because of the short Cu−N_{eq} lengths. Ferromagnetic coupling can be established when the strict orthogonality between Cu $d\sigma$ and Cr $d\pi$ orbitals is met. From Table 4, authentic ferromagnetic interaction results when the Cu−N_{eq}−C_{eq} angles are close to 180° and then S is allowed to be almost zero. In terms of orbital considerations in the current system possessing the long Cu−N_{ax} bond lengths, the magnetic orbital ($d_{x^2-y^2}$) on a Cu(II) atom is situated in the basal plane of the macrocyclic ligand. Hence, the spin density of the Cu center does not propagate efficiently through the empty π^* orbital of a CN bridge that overlaps in π symmetry with the $d\pi$ orbitals of adjacent Cr(III) atoms. The observed ferromagnetic interactions ($J > 0$) in **3** and **4** reveal that the overlap of magnetic orbitals is not sizable and the J_{AF} term becomes almost negligible, compared to J_F. Based on Table 4, the magnetic coupling in the Cr(III)Cu(II) systems with axially elongated Cu(II) units is mainly determined in terms of the Cu−N_{ax} distances, although some magnetic contributions, depending on the different Cu−N_{ax}−C_{ax} angles, may be marginally taken into account.[28]

Conclusions

We have prepared three two-dimensional (2D) layered complexes (**1**, **3**, **4**) with honeycomb-like architectures and a pentanuclear cluster (**2**) by reacting $[M(CN)_6]^{3-}$ (M = Fe, Cr) and respective Cu macrocycles. The structural variations of M(III)Cu(II) bimetallic assemblies are subject to the steric congestions arising from the pendant methyl (**1**, **3**) and ethyl (**2**, **4**) side groups on L1 and L2, respectively. Notably, the bulkiness of the ethyl groups in **2** and **4** facilitates more structural distortion along the axial directions around a Cu center, eventually bringing about the pronounced elongation associated with the very long Cu−$O(N)_{ax}$ lengths of 3.095(8) Å in **2** and 3.075(3) Å in **4**. The overall crystal packings are arranged in a way that the steric hindrance is minimized. From the structural and magnetic parameters, the Cu−N_{ax} bond length seems to be a considerable factor affecting the magnitude of magnetic couplings in the related systems.

Acknowledgment. This work was supported by the National Research Foundation of a Korea Grant funded by the Korean Government (No. 2010-0000046 and 2010-0015790).

Supporting Information Available: X-ray crystallographic files (in CIF format), and additional structural and magnetic data (PDF) for **1**−**4**. This material is available free of charge via the Internet at http://pubs.acs.org.

(34) Kou, H.-Z.; Zhou, B. C.; Gao, S.; Liao, D.-Z.; Wang, R.-J. *Inorg. Chem.* **2003**, *42*, 5604.
(35) Kahn, O. *Molecular Magnetism*; VCH: Weinheim, Germany, 1993.